Paper ID – 126 **Session 2022**
Study Committee A3
PS2 - Decarbonisation of T&D Equipment

Comparative Continuous and Overload Current Performance of High Voltage Switchgear with SF_6 and Alternative Gases

Victor HERMOSILLO
GE Grid Solutions
U.S.A.

Diana LEGUIZAMON-CABRA, Marius CATALA, Ludovic DARLES, Cyril GREGOIRE, Jean-Alain RODRIGUEZ
GE Grid Solutions
France

victor.hermosillo@ge.com, diana.leguizamon-cabra@ge.com, Marius.Catala@ge.com, ludovic.darles@ge.com, cyril.gregoire@ge.com, jean-alain.rodriguez@ge.com

SUMMARY

The introduction of SF_6 gas alternatives in High-Voltage (HV) Gas-Insulated Switchgear (GIS) requires consideration of the impact of comparatively reduced gas thermal properties affecting the equipment's continuous and overload current carrying capabilities. This topic is relevant as electric power system locations are experiencing increasing current flows associated with the addition of new generation. Equipment operating conditions are further affected by climate change, including frequent and sustained seasonal energy demand during heat waves and increases of average and peak ambient temperatures.

Results and analysis are performed for various HV gas-insulated switchgear, including GIS busbars, Live-Tank (LT) and Dead-Tank (DT) circuit breakers. The insulating gas is a $C_4FN/O_2/CO_2$ mixture which offers a solution for sustainable replacement of SF_6 for all voltage and current ratings. Equipment insulated with this gas provides favourable characteristics for environmental impact, scalability, performance, footprint, and cost. A comparative evaluation of continuous current characteristics between said gas mixture and SF_6 as well as other alternatives is presented. GIS busbar thermal behaviour is assessed through numerical simulations based on fundamental properties. Results are compared with experimental behaviour obtained on this busbar with various insulating gases at different current levels. These include increase above ambient temperature and overload coefficients. GIS busbar results are then compared with DT circuit breaker temperature rise test results for identical parameter variations. Test data is also presented for LT circuit breakers, followed by an evaluation of the impact of various breaking duties on the joule losses of the equipment for various interrupting duties. Such duties represent the effects of service conditions on the circuit breaker continuous current capability. Results demonstrate the stability of the resistance value during $C_4FN/O_2/CO_2$ gas-insulated equipment lifetime.

Comparison and evaluations are presented for gas-insulated equipment. Switchgear scalability over the existing range of current ratings is achievable with both solutions. Switchgear resistance stability during equipment lifetime is achieved with both alternatives. $C_4FN/O_2/CO_2$ and SF_6 gases ensure reliable and stable joule losses under nominal current operation. Results confirm that both technologies have similar behaviour, with small differences that can be compensated by design features for the former technology. The absence of drastic resistance changes after interrupting duty allows $C_4FN/O_2/CO_2$ gas insulated switchgear to offer significant reduction in equipment environmental impact.

KEYWORDS

Temperature rise, continuous current, gas-insulated switchgear, live-tank, dead tank, circuit breaker, fluoronitrile, gas insulation, $C_4FN/O_2/CO_2$ mixed gas, contact resistance, environmentally friendly.

1. HV GIS Busbar Simulation

Temperature rise performance of HV apparatus depends on several heat transfer mechanisms including conduction, convection, and radiation. Regarding gas involvement, convection heat transfer phenomena is the most relevant. Convection comprises the combined effects of conduction and fluid flow. The flow here is not due to any externally generated, forced convection but only due to density gradient generated by central conductor heating. This kind of convection is named "natural convection" or "free convection". In the case of an HV GIS Busbar, the raise of conductor's temperatures is mainly due to Joule effect. Conductors heat the gas inside the enclosure generating density gradients. The difference of density due to this heating is the key driving mechanism of free convection.

Usually, we consider the Nusselt number which is the ratio of convective to conductive heat transfer at the boundary of a fluid. This dimensionless number is closely related to the Raleigh number and the Raleigh Number characterises the fluid's flow regime. From laminar flow for the lower range to turbulent flow for the higher range. A first analytical assessment of each gas can help to compare the convective heat exchange properties between several gases. In this section we will compare convective heat exchange capability of SF_6, carbon dioxide and technical air.

A physical property to be considered here is the thermal effusivity *e* of a gas which is related to its ability to exchange thermal energy with its surroundings.

$$e = \sqrt{k.\rho.C_p}$$

with e : thermal effusivity [J/m² K $s^{0.5}$]
k : thermal conductivity [W/(m K)]
ρ: density [kg/m^3]
C_p : specific heat capacity [J/(kg K)]

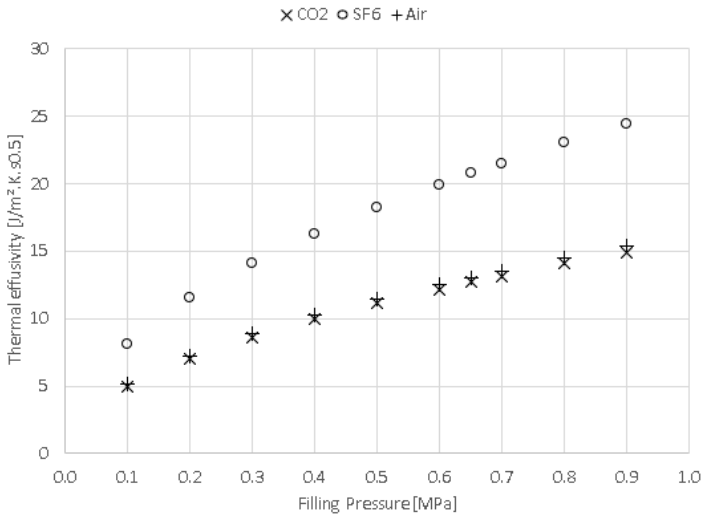

Figure 1: Thermal effusivity of CO_2, SF_6 and technical air in gaseous form over pressure

As shown by Figure 1, carbon dioxide and technical air (80% N_2/20% O_2) effusivities are very similar with respect to filling pressure. However, thermal effusivity of SF_6 is always much higher (~38%) than that of the other gases. This gap can be explained mainly by the density/molar mass difference between SF_6 and carbon dioxide or technical air. Thus, with respect to convective heat transfer, SF_6 gas performance remains much higher than that of carbon dioxide and technical air.

Increasing the filling pressure of carbon dioxide or technical air apparatuses will increase their convective heat transfer performance and reduce the difference between SF_6 and carbon dioxide or

technical air effusivities. A higher filling pressure increases effusivity, resulting in lower temperature rise values. This can be easily shown by calculation. 2D GIS Finite Element calculations were performed at several filling pressures to illustrate the effect of this parameter on temperature rise. As expected, a higher filling pressure decreases temperature rise. Performance gains are reduced at higher filling pressure values.

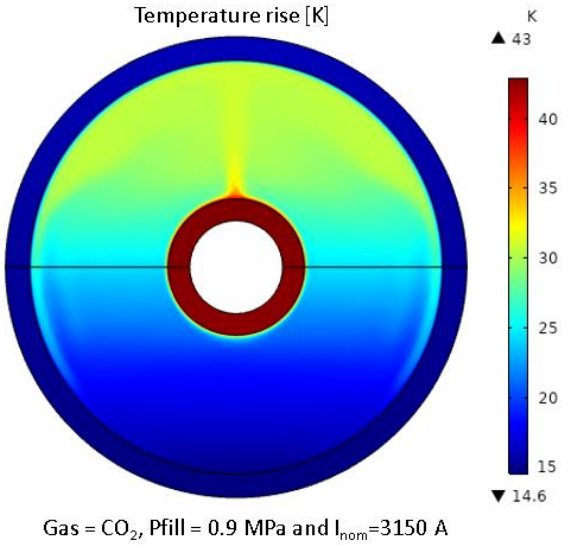

Figure 2: Temperature rise, GIS busbar 2D computation

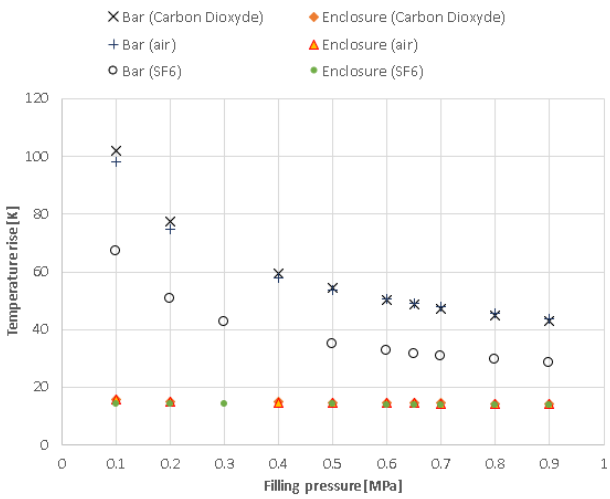

Figure 3: Temperature rise, GIS busbar

To obtain performance similar to SF_6 with carbon dioxide or air, it would be necessary to raise the filling pressure to impractical values. These results show that additional design actions are necessary to obtain equivalent performance with alternative gases. In most cases, design and conceptual changes are necessary, such as shape optimization. Boosting radiation losses when it is possible offers another improvement option. Moreover, as mentioned in [6], reducing the resistance of particular elements such as joints, connections and contact systems will have significant impact on the equipment's temperature rise performance.

2. GIS Busbar Experiments

Temperature rise experiments were carried out on a GIL mock-up at 3150 A and 4000 A with 100% of current return through the vessel. The mock-up is equipped with temperature sensors near contacts, bolted connexions, on the busbars, tanks, and insulating spacers. The busbar lengths are purposedly short (< 1 m) to investigate worst case conditions. Experience shows that longer busbars will exhibit lower temperature rise because of and the associated increase in heat exchange surface.

Two types of busbars were investigated, Type 1 is a cylindrical hollow tube and Type 2 is a modified busbar that improves heat exchange between the gas and the busbar. The experiments were also carried out with two types of spacer electrodes, named A and B. Electrode B being more cost-effective (simpler contact design) than electrode A. A summary of test results and a picture of the mock-up in the laboratory are shown in **Error! Reference source not found.** and Figure 4, respectively.

The temperature profile along busbars Type 1 and 2 at 3150 A with SF_6 and $C_4FN/CO_2/O_2$ with electrode A is shown in Figure 5. The figure shows the difference between the measured temperatures and the highest temperature in SF_6 busbar type 1. This hottest point is located on the spacer electrode and is positioned at 0 on the graph (blue curve).

Table 1: Temperature rise test summary

Test N°	Busbar	Spacer Electrode	Gas type	Gas pressure (MPa abs.)
1	1	A	SF_6	0.65
2	1	A	C_4FN (5%)/ O_2(13%)/CO_2	0.8
3	2	A	SF_6	0.65
4	2	A	C_4FN (5%) /O_2(13%)/CO_2	0.8
5	2	B	C_4FN (5%)/ O_2(13%)/CO_2	0.8
6	2	B	O_2 (13%) / CO_2 (87%)	0.8
7	2	B	Dry air	0.8
8	2	B	Dry air	0.9

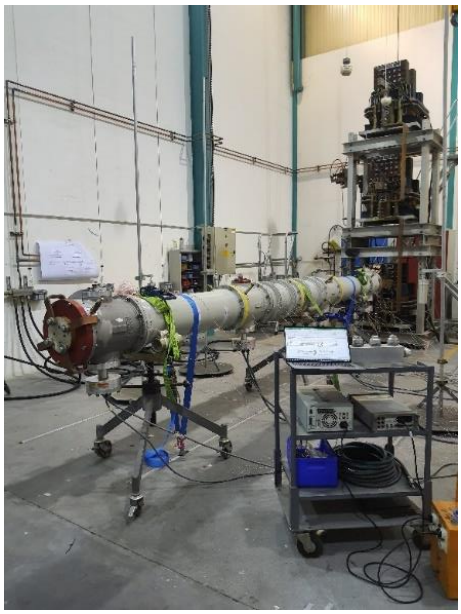

Figure 4– Picture of GIL under test

For the same busbar Type 1, the temperature with $C_4FN/O_2/CO_2$ mixture is 6.7 K° higher because of its lower thermal capabilities compared to SF_6. This difference is consistent with previous reported values [1]. The improvement of thermal design with busbar Type 2 decreases the temperature by 8 K° in the middle of the busbar and by 7 K° on the spacer's electrode. This improvement brings the thermal performance of $C_4FN/O_2/CO_2$ mixture at the same level as SF_6 for the hottest point.

Details of temperature profile are detailed for 3150 A. Experiments at 4000 A will not be commented in this paper as they generally resulted in the same conclusions. The results will only be used to assess the overload coefficients values.

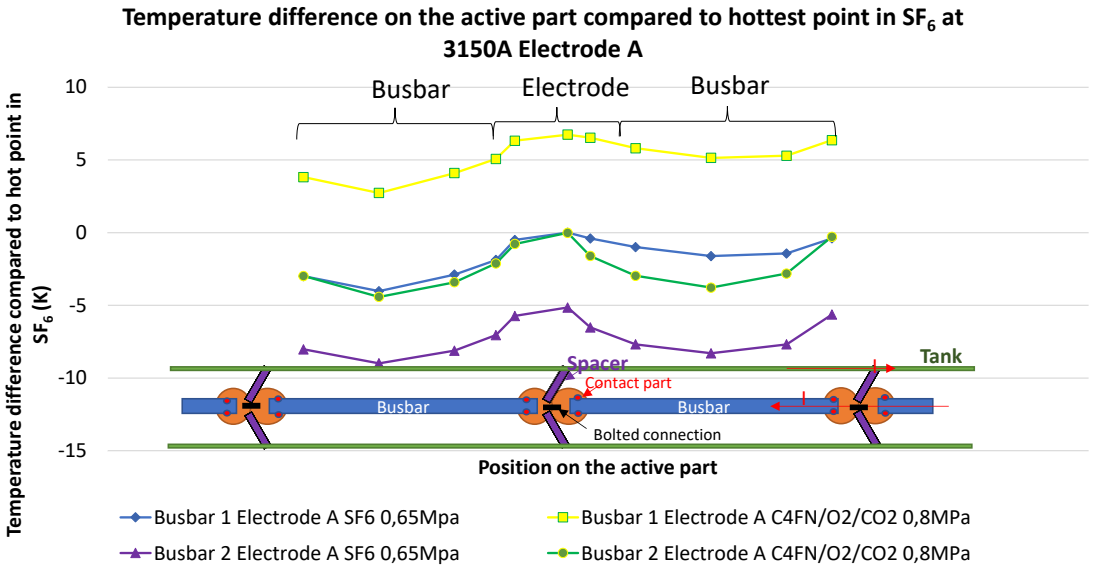

Figure 5 – Temperature profile along busbar Type 1 and 2, Electrode A, at 3150 A with SF_6 and $C_4FN/O_2/CO_2$ mixture

With Electrode B, Type 2 busbar was tested with $C_4FN/O_2/CO_2$, CO_2/O_2 mixture and (N_2/O_2, 80/20%) technical air. Results are shown in Figure 6. The highest temperatures are obtained with technical air at 0.80 MPa abs where the temperature of the contacts is 4 K° higher than the same pressure with $C_4FN/O_2/CO_2$. CO_2/O_2 at 0.80 MPa abs and Dry air at 0.90 MPa abs temperatures are 2 K° higher than $C_4FN/O_2/CO_2$ mixture. The impact of C4FN is therefore quite limited regarding temperature rise with a small impact of 2 K° reduction when adding 5% C_4FN in a CO_2/O_2 mixture at the same pressure.

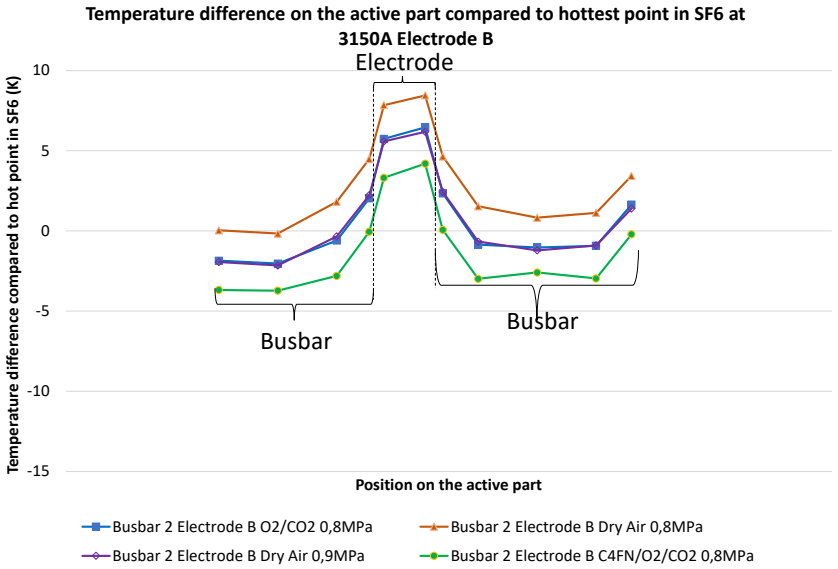

Figure 6 – Temperature profile along busbar Type 2, Configuration B, at 3150 A with SF_6 alternative mixtures.

The temperature on the tanks at different positions compared to the hottest point in SF_6 is plotted in Figure 7 for 3150 A. Results are shown for tests N° 1 to 4. The highest temperature in these cases is in the middle of the tank. Because busbar Type 2 improves the heat exchanges between the busbar and the gas, the heat is better conveyed to the tank and its temperature increases slightly. The increase is about 1 K°.

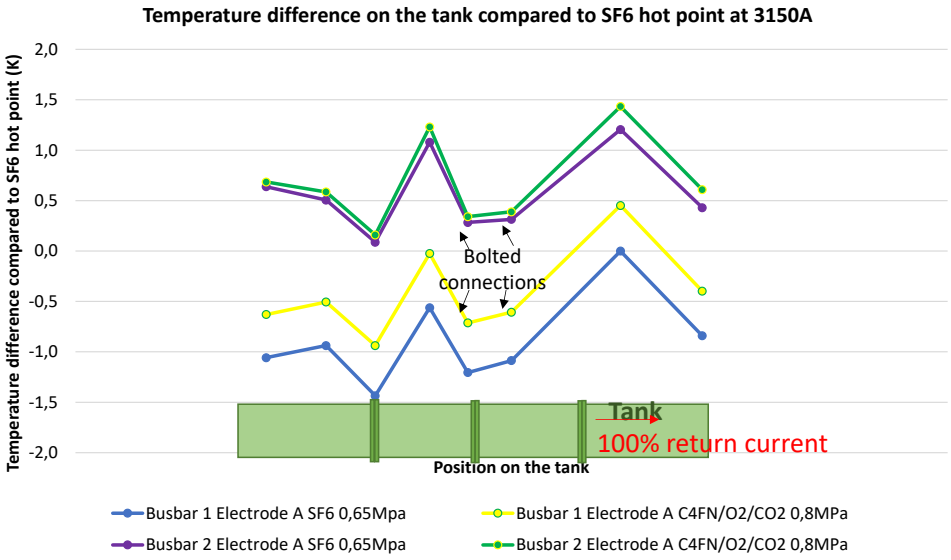

Figure 7 – Temperature profile along the tank with busbar Type 1 and 2, Electrode A, at 3150 A with SF_6 and $C_4F_7N/CO_2/O_2$ mixture

The overload coefficients α for SF_6 and $C_4FN/CO_2/O_2$ mixture are calculated with the following equation [7]:

$$\theta_a = \theta_{max} - (\frac{I_a}{I_r})^{\alpha} * \theta_r$$

with

I_a is the allowable continuous load current at actual ambient temperature θ_a [A]
I_r is the rated normal current [A]
θ_{max} is the allowable hottest spot total temperature (θ_{max} =θ_r + 40) [°C]
θ_r is the allowable hottest spot temperature rise at rated normal current [K°]
θ_a is the allowable or actual ambient temperature, in °C.

Table 2 shows the overload coefficients for the main parts which are very similar for $C_4FN/CO_2/O_2$ and SF_6. Moreover, the change of busbar type does not significantly change the values for inner parts and enclosures.

Table 2: Overload coefficients on different parts for SF_6 and $C_4FN/CO_2/O_2$ mixture

	Electrodes	**Busbar**	**Tank**
θ Type 1 busbar SF_6	1,68	1,71	1,84
θ Type 2 busbar SF_6	1,71	1,70	1,82
θ Type 1 busbar C4FN / CO_2 / O_2 mixt.	1,69	1,68	1,85
θ Type 2 busbar C4FN / CO_2 / O_2 mixt.	1,71	1,71	1,82

3. Dead Tank experiment

Temperature rise experiments were carried out on a DT circuit breaker rated 145 kV at nominal currents between 3000 A and 4000 A (Figure 8). The mock-up is equipped with temperature sensors on contacts, silver coated parts, bolted connexions, over the central conductor and tank as per IEEE C37.04-2018. Comparative tests were done between $C_4FN(3.5\%)/O_2$ (13%)/CO_2 (83.5%) gas mixture (C_4FN mixture) and SF_6 gas.

Figure 8 Picture of Dead Tank circuit breaker rated 145 kV under test.

Various configurations were tested at various continuous currents as described in Table 3. Measuring points along the interrupting chamber and bushings are indicated in Figure 9. The differences between temperature rise measurements with $C_4FN/CO_2/O_2$ mixture at different positions and the hottest point in SF_6 are plotted in Figures 10 to 13 for currents of 3000 A and 4000 A.

Table 3: Dead tank circuit breaker configurations and currents during test.

	3000 A	**3300 A**	**3500 A**	**4000 A**
Bushing	Composite	Composite	Composite	Composite
Central conductor	Solid aluminium	Solid aluminium	Solid copper	Solid copper
Ambiant temperature	25°C	25°C	25°C	25°C
Gas & pressure	C_4FN mixture 0.85 MPa abs SF_6 0.61 MPa abs	C_4FN mixture 0.85 MPa abs	C_4FN mixture 0.85 MPa abs	C_4FN mixture 0.85 MPa abs SF_6 0.61 MPa abs

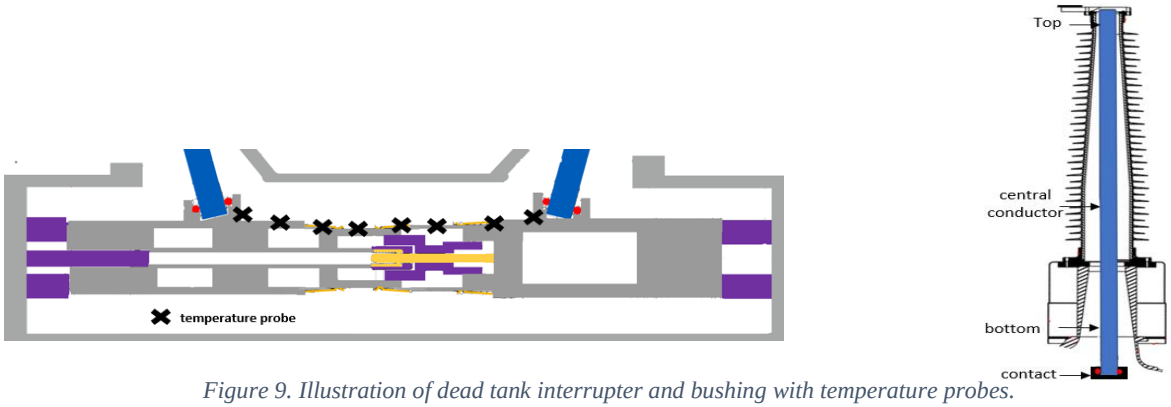

Figure 9. Illustration of dead tank interrupter and bushing with temperature probes.

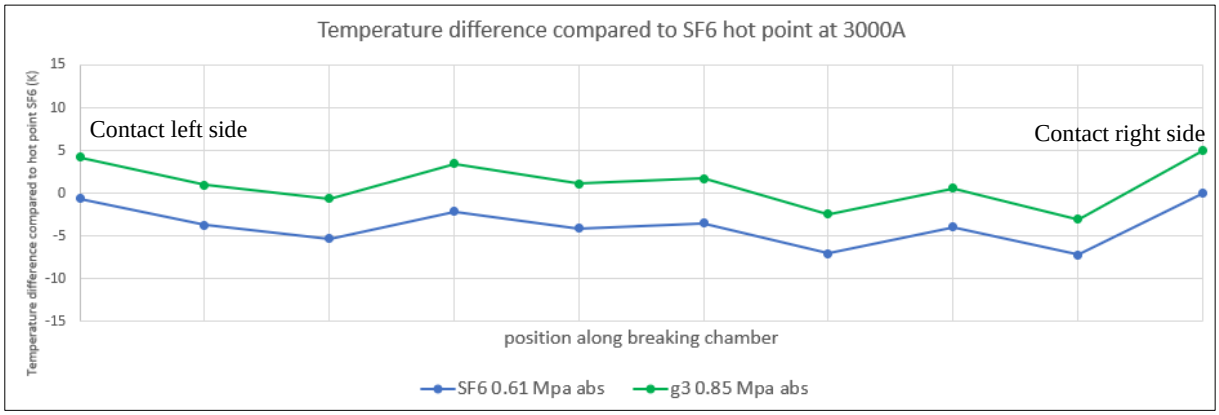

Figure 10. Temperature profile along the breaking chamber at 3000 A with SF_6 and $C_4FN/CO_2/O_2$

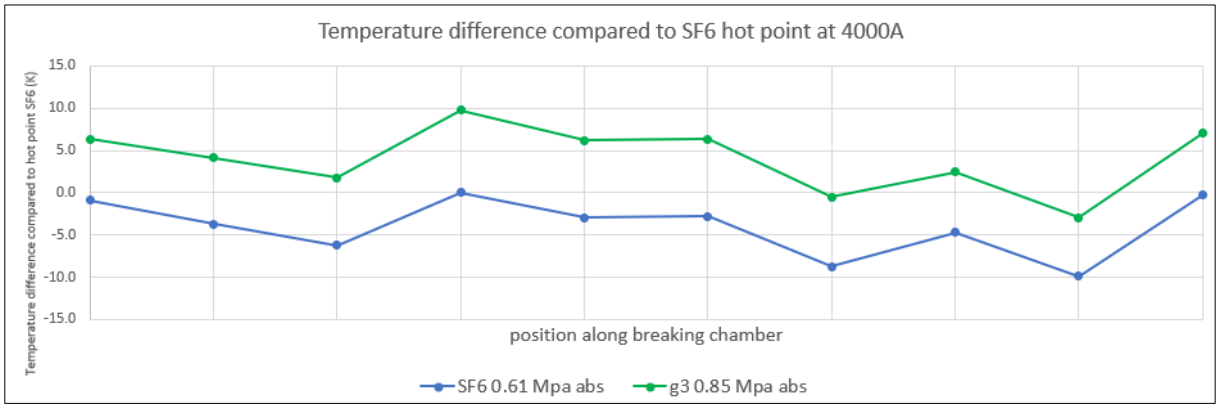

Figure 11. Temperature profile along the breaking chamber at 4000 A with SF_6 and $C_4FN/CO_2/O_2$

The temperature profiles for the interrupting chamber at 3000 A and 4000 A, in Figures 10 and 11, are nearly parallel. Thus, the temperature elevation between SF_6 and $C_4FN/CO_2/O_2$ cases is nearly constant regardless of the interrupter component material, its finish or the kind of connections (inserted, bolted or pressed).

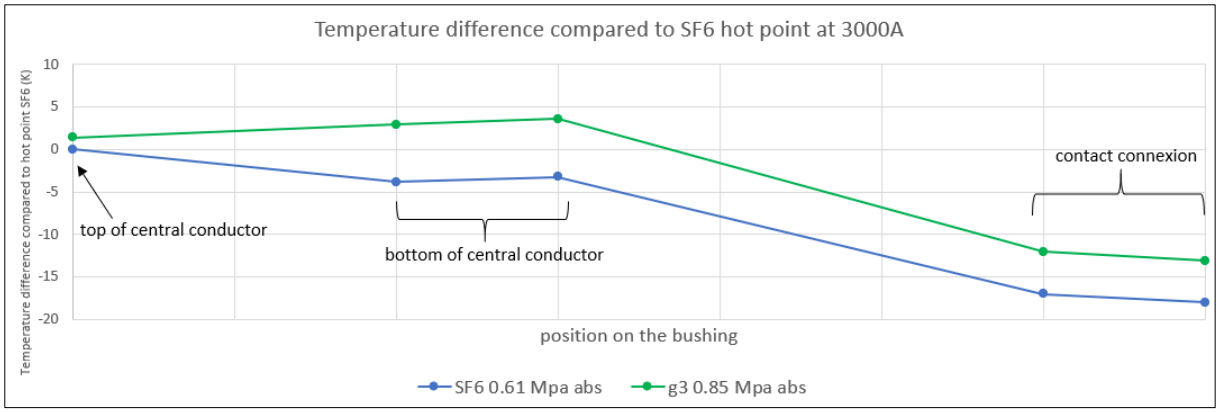

Figure 12. Temperature profile along the bushing at 3000 A with SF_6 and $C_4FN/CO_2/O_2$

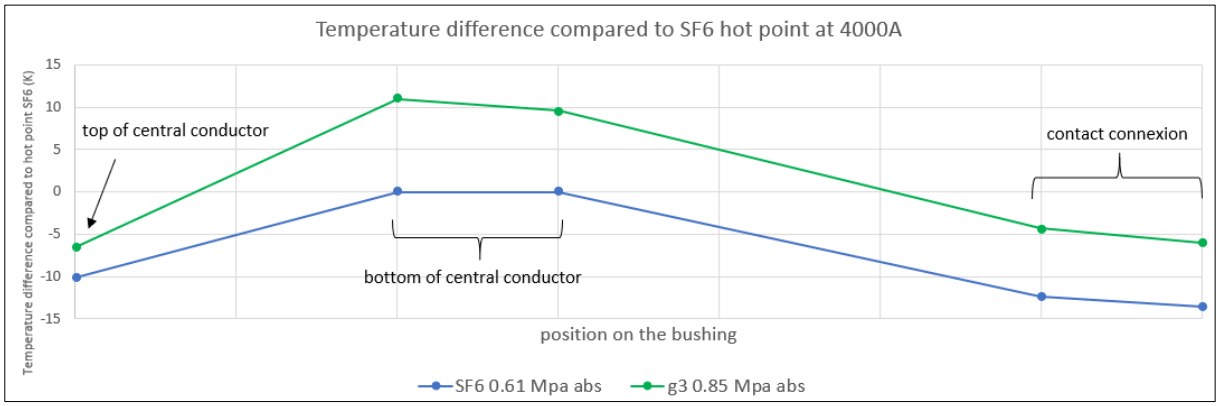

Figure 13. Temperature profile along the bushing at 4000 A with SF_6 and $C_4FN/CO_2/O_2$

For the bushing conductor temperature measurements at 3000 A and 4000 A in Figures 12 and 13, the hottest point is localized on the bottom of the central conductor. This can be explained by a limitation of contact design or number of contacts between central conductor and breaking chamber. With a different contact type or dimensioning, the hottest point may be shifted back to the top of the bushings.

Glass transition in the composite insulator top flange glue joint was checked at 3000 A and 4000 A. Temperature rise difference between $C_4FN/CO_2/O_2$ and SF_6 was about 3.5 K, remaining much below the glue glass-transition temperature.

Table 4 shows the overload coefficient for breaking chamber and bushing. $C_4FN/CO_2/O_2$ mixture does not change the overload coefficient α as defined in the formula 1 with similar values as SF_6 gas [3].

Table 4: Overload coefficients on different parts for $C_4FN/CO_2/O_2$ mixture

$C_4FN/CO_2/O_2$ 3000-3300 A	α	ΔT_{max} calculated - measured
Breaking chamber	1,82	0.3 K
Bushing with central conductor		0.7 K

$C4FN/CO_2/O_2$ 3500-4000 A	α	ΔTmax calculated - measured
Breaking chamber	1,71	0.3 K
Bushing with central conductor		4.7 K

4. Variation of Contact Resistance with Electrical Wear in $C_4FN/CO_2/O_2$ Circuit-Breaker

During the homologation campaign according to the IEC standard 62271-100 for the first gas-insulated Live Tank (LT) circuit breaker rated 145 kV, 40 kA, using a C_4FN (3.5%)/ O_2 (13%)/ CO_2 gas mixture, the main circuit contact resistance was measured between terminals before and after the tests.

An LT circuit breaker arrangement was selected as the test object for such measurements because the contribution of the breaking unit to the overall contact resistance is more significant (contrary to GIS or Dead tank circuit breaker where the interrupter unit contribution to changes after interrupting duties is more limited in relation to the overall resistance). About 70% of the terminal-to-terminal resistance in a DT circuit breaker is associated with its two bushing conductors. The following chart is presenting the results obtained with a measurement DC current of 200 A applied on the terminal plates highlighted by the red circles on the picture attached.

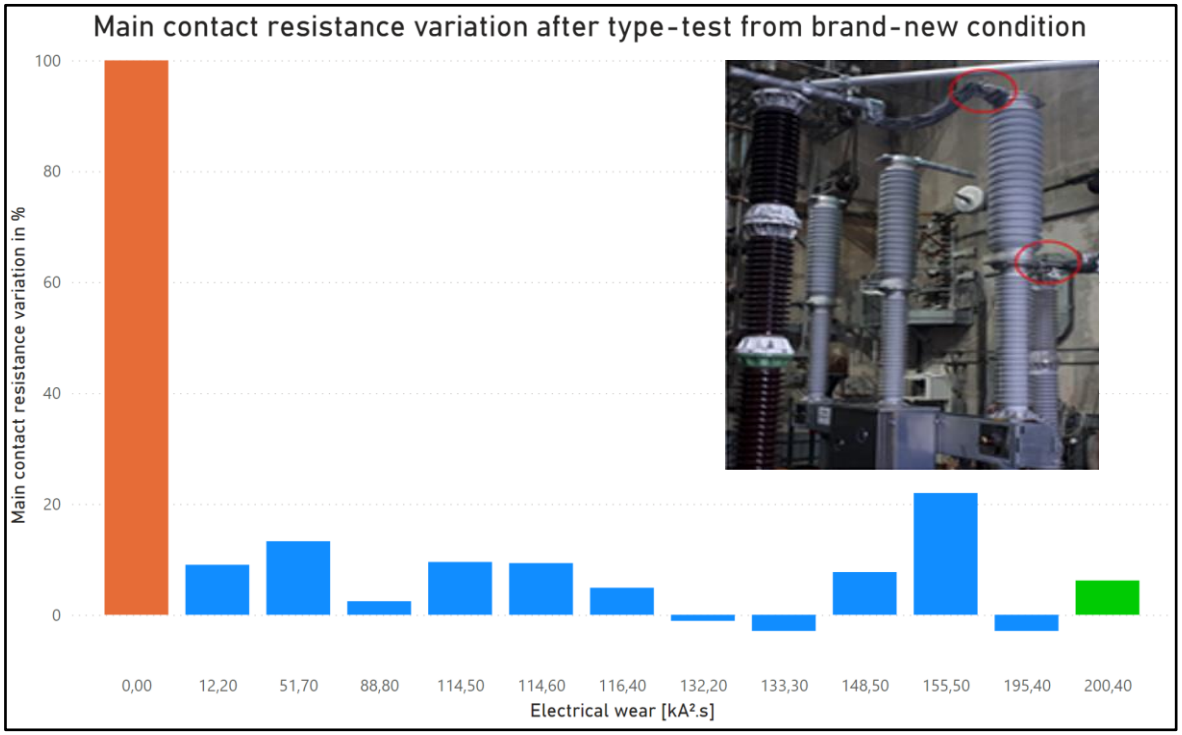

Figure 9 : Main contact resistance variation after type-test from brand new-condition

In the applicable standard [4] §7.4.4.2, the resistance condition check is considered satisfactory if the resistance increase for each phase is not greater than 100%. This limit is depicted in the chart in Figure 9 by an orange bar. Blue bars represent resistance measurements performed after different type-tests during the homologation campaign with the associated wear represented by the cumulative interrupted current in $kA^2.s$. Based on these tests, it was determined that there is no direct link between the wear level of the circuit-breaker and the resulting contact resistance change. Variations are mostly related to parts tolerances in the assembly as in SF_6 gas circuit-breakers.

Finally, the green rectangle is a measurement of the highest wear test where the main contact resistance has been assessed one year after the test with the breaker remaining exposed to $C_4FN/CO_2/O_2$ arced gas mixture. The objective was to detect if wear or decomposition product of Fluoronitrile-based solution could influence the main contact resistance along the time. The result of this specific test being in the range of the others, it can be concluded that the main contact resistance will only see minor modification of its value after breaking operations and will not vary overtime due to any ageing phenomena.

A large contact resistance increase on a LT breaker would correspond to a significant damage of the main contact path integrity and may compromise the current carrying capability of the switchgear by generating possible runaway temperature rise issues as the increase of contact resistance is generally concentrated on a limited number of contact points. Care shall be taken to limit the contact resistance increase at the design stage. In this regard, contact resistance variation currently allowed in applicable standards seems too high for type tests (i.e.: today: +100% allowed in IEC [4], +250% allowed in IEEE [5]). In contrast, field conditions and equipment ageing may lead to higher contact resistance increase than type tests due, for example, to contact pressure reduction (loosening) as a result of a high number of mechanical operations, and oxidation due to acidification.

5. Conclusions

The current carrying capability was investigated for different alternatives to SF_6 and different HV switchgear applications (Gas Insulated Line and DT circuit-breaker). The results of the experiments are in accordance with simplified CFD model simulations which shows temperature rises which are very closely related to the thermal effusivity of each gas or gas mixture. SF_6 has a lower temperature rise compared to its alternatives. However, as the operating pressures of SF_6 alternatives are generally higher, part of that difference is recovered. Nevertheless, a moderate increase in the temperature rise is observed with $C_4FN/CO_2/O_2$ gas mixture compared to SF_6. As a comparison, for the same pressure and test object, slightly higher temperature increase is observed with technical air or CO_2/O_2 mixture compared to $C_4FN/CO_2/O_2$. In parallel, it is established that the change of gas leads to negligible variation of the temperature rise on the enclosures. Small design adaptations allow to recover the nominal current capability keeping the same footprint between SF_6 and $C_4FN/CO_2/O_2$ gas mixture.

Additionally, the usual average overload coefficient of 1.8 considered for SF_6 applications is also found as valid for $C_4FN/CO_2/O_2$ gas mixture for dead tank and GIS equipment.

Finally, when comparing the main current path resistance in new and after a complete lifetime of switching, no significant differences can be measured, demonstrating the stability of the main current path resistance in switchgear throughout its entire lifetime. This ensures reliability, stable nominal current performance and no increase of joule losses which is key to guarantee a limited climate impact of the apparatus during its use phase.

BIBLIOGRAPHY

[1] Y. Kieffel, F. Biquez, P. Ponchon and T. Irwin, "SF_6 alternative development for high voltage Switchgear," 2015 IEEE Power & Energy Society General Meeting, 2015, pp. 1-5, doi: 10.1109/PESGM.2015.7286096.

[2] CIGRE Working Group SC 22-12, “The thermal behaviour of overhead conductors Section 1 and 2 Mathematical model for evaluation of conductor temperature in the steady state and the application thereof” (Electra number 144 October 1992 pages 107-125).

[3] IEC TR 62271-306: High-voltage switchgear and controlgear – Part 306: Guide to IEC 62271-100, IEC 62271-1 and other IEC standards related to alternating current circuit-breakers.

[4] IEC 62271-1 - Edition 3.0 2021 – “High-voltage switchgear and controlgear – Part 1: Common specifications for alternating current switchgear and controlgear.”

[5] IEEE C37.04-2018, “IEEE Standard Test Procedures for AC High-Voltage Circuit Breakers with Rated Maximum Voltage Above 1000 V.”

[6] CIGRE Technical Brochure 830: “Application and Benchmark of Multiphysics Simulation Tools for Temperature Rise Calculations”, 2021.

[7] IEC TR 62271-306 - Edition 1.1 2018-08 - High-voltage switchgear and controlgear – Part 306: Guide to IEC 62271-100, IEC 62271-1 and other IEC standards related to alternating current circuit-breakers.